Journal of Membrane Science 760 (2026) 126220

Contents lists available at ScienceDirect

Journal of Membrane Science

journal homepage: www.elsevier.com/locate/memsci

Commercial polymer-supported ultrapermeable NaA zeolite membrane towards high-efficiency hydrogen purification

Shijie Yang [a], Jiahong Pan [b,*], Yi Liu [a,**], Shengyan Meng [a], Hongyan Xiao [a], Yunlei Gao [a], Junze Li [a], Weijun Xu [a], Minxiu Zou [a], Meng Ge [a], Rongfei Zhou [c], Yi Liu [a,***]

[a] State Key Laboratory of Fine Chemicals, Frontiers Science Center for Smart Materials, School of Chemical Engineering, Dalian University of Technology, Dalian, 116024, China
[b] International Joint Center of Nature-Inspired Carbon Neutrality Solutions, School of Resources, Environment and Materials, Guangxi University, Nanning, Guangxi, 530004, China
[c] State Key Laboratory of Materials-Oriented Chemical Engineering, College of Chemical Engineering, Nanjing Tech University, Nanjing, 210009, China

ARTICLE INFO

Keywords:
Zeolite membranes
Polyethersulfone
Gas separation
Hydrogen purification
Cost-benefit analysis

ABSTRACT

Zeolite membranes have demonstrated great potential in high-efficiency H_2 purification. Nonetheless, their reliance on expensive and brittle inorganic supports severely hinders industrial applications. In this study, we prepared well-intergrown NaA zeolite membranes on low-cost commercial porous polyethersulfone (PES) supports through mild epitaxial growth, which was of vital importance for maintaining excellent interfacial strength between NaA zeolite layers and supports. Owing to low diffusion resistance of PES supports and their strong adhesion with NaA zeolite layers, our membranes exhibited ultrahigh H_2 permeance of 2.6×10^{-6} mol m^{-2} s^{-1}·Pa^{-1} with excellent separation factors for equimolar H_2/CO_2 (15.7) and H_2/CH_4 (14.7), which was superior to the majority of reported ceramic-supported counterparts. A comprehensive cost-benefit analysis further indicated that compared with conventional porous α-Al_2O_3 supports, a total fabrication cost reduction up to 99.2% in terms of H_2 purification could be achieved, providing a compelling pathway for their batch production.

1. Introduction

As a clean and efficient energy carrier, hydrogen energy is playing an increasingly important role in global energy transition [1–4]. However, cost-efficient production of high-purity H_2 from CO_2 and CH_4-containing industrial off-gases [5,6], such as steam methane reforming (SMR) off-gas, remains a major bottleneck for its wide application such as fuel cells [7–13]. While pressure swing adsorption technology has been widely used in H_2 purification, it still suffers from high energy consumption and capital cost. Alternatively, membrane technology [14–16] has been considered as a promising candidate for high-efficiency H_2 purification due to its low energy consumption, simple operation, and compact footprint [17–19].

In recent decades, zeolite membranes have shown great promise for high-efficiency gas separation, owing to their uniform pore size and rich functional groups [20]; in particular, zeolites commonly possess superior thermal, mechanical, and chemical stability, rendering them robust under harsh conditions [21–28]. Among them, NaA zeolites, possessing an effective aperture size of 0.42 nm and a highly polar framework rich in sodium cations, represent an ideal candidate for separating smaller-sized H_2 molecules (0.29 nm) from other larger-sized gas molecules such as CO_2 (0.33 nm), N_2 (0.36 nm), and CH_4 (0.38 nm) based on molecular sieving and competitive adsorption mechanisms [29]. In recent decades, considerable efforts have been devoted to fabricating NaA zeolite membranes for high-efficiency H_2/CO_2 separation. For instance, Huang et al. pioneered the fabrication of neutral and cation-free LTA-type aluminophosphate ($AlPO_4$) molecular sieve membrane on porous α-Al_2O_3 support, exhibiting an ideal H_2/CO_2 selectivity of 10.9 [30]. Varela-Gandía et al. fabricated ion-exchanged Na-LTA zeolite membrane on macroporous carbon support through epitaxial growth. Fine-tuning of effective pore size via alkaline cation exchange was found to facilitate H_2 separation from H_2/CO mixtures towards PEM

* Corresponding author.
** Corresponding author.
*** Corresponding author.
E-mail addresses: jhpan@gxu.edu.cn (J. Pan), liuyichem@jlu.edu.cn (Y. Liu), diligenliu@dlut.edu.cn (Y. Liu).

https://doi.org/10.1016/j.memsci.2026.126220
Received 19 August 2026; Received in revised form 17 September 2026; Accepted 25 September 2026
Available online 3 October 2026
0376-7388/© 2026 Elsevier B.V. All rights are reserved, including those for text and data mining, AI training, and similar technologies.

fuel cell applications [31]. Their competence in high-efficiency H_2 purification has also been demonstrated by other recent studies [30–35].

Despite significant progress made in fabricating high-performance zeolite membranes, the use of expensive and brittle ceramic supports [27,36–38], accounting for the majority of production costs of zeolite membranes (>70%) [39], remains a major bottleneck towards their industrial applications; simultaneously, excessive diffusion resistance arising from ceramic supports commonly results in lower gas permeance [40–42]. To address the above concerns, commercial polymers have emerged as ideal candidate of supports for zeolite membranes, owing to their intrinsic advantages such as low cost, mechanical flexibility, and high porosity [43–45]. Nevertheless, compared with ceramics, their inferior thermal and mechanical stability as well as weak affinity with zeolite crystallites necessitate specific synthetic strategies. For instance, prior to hydrothermal synthesis, Ge et al. pre-embedded zeolite "anchors" within polymer matrix, resulting in the formation of a robust polymer-zeolite interface [43]. Recently, Deng et al. synthesized crack-free ZSM-5 zeolite membranes on custom-synthesized PTFE supports, exhibiting ultrahigh He permeance as well as high SF for He/N_2 and He/CH_4 gas pairs [46]. In spite of remarkable achievements, significant economic and technical hurdles regarding their scalable manufacturing remain to be solved [47]. For instance, aiming at maintaining excellent interfacial compatibility and structural stability, customized (e.g., polymer-zeolite composite fibers) [43] or specialized supports (e.g., PTFE) represent dominant production costs during membrane processing [46,48], inevitably negating the primary advantage of polymer supports. In terms of commercial off-the-shelf supports, it remains a formidable challenge to overcome the conflict between infiltration depth (i.e., gas permeance) and interfacial adhesion (i.e., gas selectivity), resulting in the necessity of additional post-synthetic steps to plug non-selective pinholes [49]. The above bottleneck stems from the inherent incompatibility between zeolite crystallites and commercial low-cost polymer supports. To meet this challenge, on the one hand, the adopted polymer supports should possess excellent thermal and mechanical stability as well as abundant surface functional groups; on the other hand, mild synthetic protocols should be employed to ensure the robustness of the polymer matrix during membrane processing.

Polyethersulfone (PES), which is commercially available at low cost, represents a promising candidate of zeolite membrane supports. On the one hand, it possesses excellent textural properties such as high porosity, smooth surface, and rich functionality; on the other hand, it exhibits exceptional thermal, chemical, and mechanical stability. The above advantages are expected to achieve an elegant balance between separation performance and production cost. In this study, we pioneered the fabrication of PES-supported NaA zeolite membranes through mild epitaxial growth. Among various synthetic factors, deposition of uniform seed layer via vacuum hot-drop coating was found crucial for the formation of NaA zeolite membrane with optimized microstructure. Gas permeation results indicated that as-prepared membrane exhibited ultrahigh H_2 permeance of 2.6×10^{-6} mol m^{-2} s^{-1}·Pa^{-1} as well as excellent SF of H_2/CO_2 (15.7) and H_2/CH_4 (14.7), which was superior to the majority of reported ceramic-supported counterparts. An economic analysis further demonstrated a significant cost reduction of up to 99.2% compared with ceramic-supported counterparts, highlighting their great potential in large-scale production and application.

2. Experimental section

2.1. Reagents and materials

Sodium hydroxide (NaOH, ≥ 98%), tetramethylammonium hydroxide (TMAOH, 25 wt% aqueous solution), aluminum isopropoxide (AIP, ≥99.8%), and sodium metaaluminate ($NaAlO_2$, reagent grade) were purchased from Macklin Inc. (Shanghai, China). Colloidal silica (LUDOX® AS-40, 40 wt% suspension in H_2O) was supplied by Sigma-Aldrich (USA). Porous polyethersulfone (PES) supports (pore size: 0.22 μm; diameter: 25 mm) were obtained from Shanghai Feiling Biotechnology Co., Ltd. (Shanghai, China). All chemicals were used as received without further purification. Deionized (DI) water was used throughout all experiments.

2.2. Preparation of NaA zeolite seeds

The molar composition of the seed synthesis solution was 0.32 Na_2O: 1 Al_2O_3: 3.92 SiO_2: 4.31 $(TMA)_2O$: 340H_2O. Initially, 0.13 g of NaOH was dissolved in 17 mL of DI water, followed by the addition of 16 mL of TMAOH aqueous solution. The resulting mixture was then heated in a water bath and maintained at 60 °C. Subsequently, 2.08 g of AIP was added under vigorous stirring until complete dissolution. After cooling to room temperature, 3 g of colloidal silica suspension was added dropwise. The mixture was vigorously stirred for 3 h, followed by aging for 12 h. Finally, the aged solution was transferred into a Teflon-lined autoclave for hydrothermal treatment at 100 °C for 12 h. The obtained white precipitates were collected by centrifugation, washed repeatedly with DI water, and dried at 80 °C overnight.

2.3. Deposition of NaA zeolite seed layer

Vacuum-assisted hot-drop coating was employed to deposit a uniform NaA zeolite seed layer on commercial PES support. Initially, a 0.5 wt% seed suspension was prepared by uniformly dispersing as-prepared NaA zeolite seeds in DI water. The suspension was vigorously stirred for 3 days, followed by ultrasonication for 30 min prior to the formation of a homogeneous dispersion. In terms of the coating process, the PES support was placed on a vacuum filtration apparatus and pre-heated to 90 °C. Subsequently, with the vacuum supplied by a diaphragm pump, 0.2 mL of the seed suspension was added dropwise onto the support surface. After complete solvent removal, the seeded support was carefully removed and placed in a custom-made PTFE holder. Finally, the seeded support was dried in an oven at 70 °C overnight before further use.

2.4. Epitaxial growth of NaA zeolite membrane

The molar composition of the membrane growth solution was 1 Al_2O_3: 3.6 SiO_2: 50 Na_2O: 1200H_2O. The precursor solution for epitaxial growth was prepared as follows: 5.0 g of NaOH and 0.42 g of $NaAlO_2$ were dissolved in 25 g of DI water and stirred until the formation of a clear solution. Simultaneously, 5.0 g of NaOH was dissolved in 25 g of DI water, where 1.36 g of colloidal silica was added dropwise with stirring until the formation of a clear solution. Subsequently, the silicate source was slowly added to the aluminate source under vigorous stirring, followed by aging at room temperature for 12 h. During epitaxial growth, the seeded PES support, held within the custom-made PTFE holder, was placed vertically into a Teflon-lined autoclave. The aged synthesis solution was then poured into the autoclave. Hydrothermal synthesis was conducted in an oven at 80 °C for 5 h. After the reaction, the as-prepared membrane was retrieved, rinsed thoroughly with DI water, and finally dried at 50 °C for 48 h.

3. Results and discussion

3.1. Fabrication of NaA zeolite membranes

The process for fabricating PES-supported NaA zeolite membrane is schematically illustrated in Fig. 1. Initially, vacuum hot-drop coating was employed to deposit a uniform NaA zeolite seed layer on porous PES support. Among various factors, coating temperature and seed content in suspension were found to play vital roles in regulating the seed layer morphology (Fig. S1). Since the deposition process was governed by a dynamic competition between vacuum-driven infiltration and thermally induced evaporation, during vacuum hot-drop coating, the solvent was



Fig. 1. Schematic illustration of the mild fabrication of PES-supported NaA zeolite membrane.

rapidly removed, rendering uniform and compact arrangement of NaA zeolite seeds on the support surface; simultaneously, some seeds were partially embedded into the PES support pores, enabling the formation of firmly attached seed layer. This unique interfacial architecture is anticipated to mitigate uncontrolled capillary-driven infiltration while establishing a robust physical interlock between the rigid zeolite layer and the flexible polymer matrix. Subsequently, the seeded support was epitaxially grown into a well-intergrown NaA zeolite membrane under mild conditions. Owing to the low mass-transfer resistance of the PES support, the resulting membrane provides high H_2 permeance; simultaneously, benefiting from the robust physical interlock and the intrinsic flexibility of the PES support, it retains stable H_2/CO_2 separation performance after repeated bending (Fig. 1).

We first investigated the morphology of pristine PES support. As shown in Fig. 2a, the support exhibited a sponge-like porous surface comprising uniform interconnected pores. Together with the nominal pore size of 0.22 μm and thin flexible geometry as shown in Fig. S2, such textural properties were ideal to form interlocked structure during vacuum hot-drop coating. Relevant XRD pattern (Fig. 3a) indicated that bare PES support exhibited a broad amorphous hump centering at 2θ value of 18°, confirming its amorphous structure, while the FT-IR spectrum (Fig. 3b) displayed characteristic peaks assignable to the stretching vibration of O═S═O groups, thus validating the chemical composition of bare PES support. Considering the employment of water as solvent for seed suspension, wettability of the support surface was investigated by contact angle experiment. As shown in Fig. 2b, the PES support exhibited excellent hydrophilicity and rapid wetting behavior, as evidenced by instant permeation of water droplets into the matrix (Fig. S3). The intrinsic superhydrophilicity of PES support is advantageous for ensuring the formation of strongly adhered seed layer, since not only uniform and full seed suspension coverage on the support surface but also facilitated embedding of NaA zeolite seeds inside the support pores can be guaranteed under vacuum hot-drop coating.

Subsequently, NaA zeolite seeds were synthesized through hydrothermal growth. As shown by STEM (Fig. S4), obtained seeds exhibited well-defined cubic geometry with an average size of ~300 nm, while their phase purity could be further confirmed by relevant XRD pattern (Fig. 3a) and FT-IR spectrum (Fig. 3b) with characteristic bands located at ~1000 cm^{-1} (Si-O-T) and ~550 cm^{-1} (d4r). Regarding gas adsorption properties, the N_2 adsorption-desorption isotherm of the NaA seeds revealed a typical type-I isotherm with a maximum N_2 uptake of ~188 $cm^3\ g^{-1}$ at 77 K (Fig. S5), and the BET surface area was calculated to be 550 $m^2\ g^{-1}$; simultaneously, the CO_2 adsorption isotherm displayed a steep and high-capacity uptake reaching ~120 $cm^3\ g^{-1}$ (5.34 mmol g^{-1}) at 298 K and 1 bar (Fig. S6), further verifying their open microporous structure and strong CO_2 affinity.

In the next step, vacuum-assisted hot-drop coating was carried out to deposit uniform seed layer. As shown in Fig. 2c, after coating under optimized experimental conditions, the support surface had been uniformly covered with a densely packed seed layer (Fig. S1) with characteristic diffraction peaks derived from LTA zeolite phase easily distinguishable from amorphous phase (Fig. 3a). Adopting such morphology not only avoided exposure of macropores of the PES support but also provided abundant nucleation sites for epitaxial growth, facilitating the formation of well-intergrown NaA zeolite membrane.

Finally, epitaxial growth was conducted to seal the open space in seed layer. The seeded PES support was fixed in a custom-designed PTFE holder (Fig. S7), which was designed to prevent the lightweight support from floating during epitaxial growth. As shown in Fig. 2d, a well-intergrown NaA zeolite layer was readily formed on the PES support under optimized reaction conditions. Cross-sectional SEM image (Fig. 2e) confirmed that the thickness of as-prepared NaA zeolite layer reached 3.4 μm with a clearly distinguishable interface between the zeolite layer and polymer matrix. Relevant XRD pattern (Fig. 3a) confirmed the formation of highly crystalline NaA zeolite layer as evidenced by sharp increase of NaA zeolite peak intensity compared with

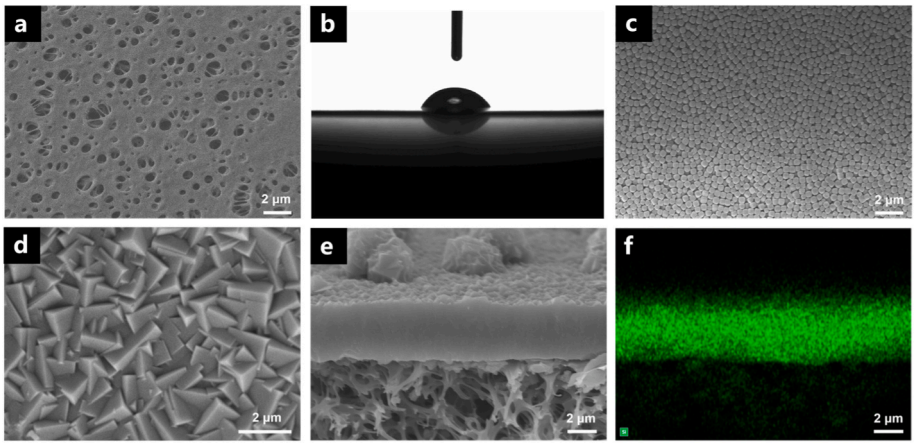


Fig. 2. (a) SEM image of bare PES support. (b) Water contact angle of bare PES support. SEM images of (c) NaA zeolite seed layer and (d, e) PES-supported NaA zeolite membrane. (f) Cross-sectional EDX mapping of Si element of PES-supported NaA zeolite membrane.

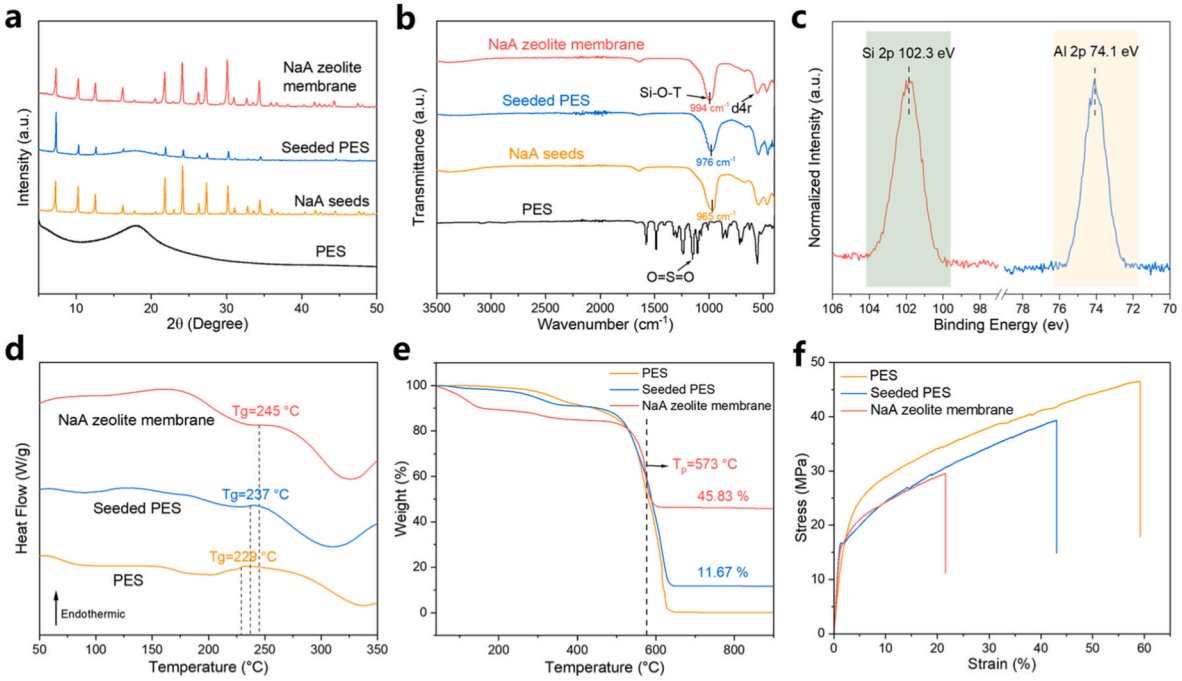


Fig. 3. (a) XRD patterns and (b) FT-IR spectra of bare PES support, NaA zeolite seeds, NaA zeolite seed layer, and PES-supported NaA zeolite membrane. (c) High-resolution XPS spectra of Si 2p and Al 2p of PES-supported NaA zeolite membrane. (d) DSC curves, (e) TGA curves, and (f) stress-strain curves of bare PES support, NaA zeolite seed layer, and PES-supported NaA zeolite membrane.

that of PES amorphous hump. As expected, FT-IR spectra (Fig. 3b) displayed characteristic peaks derived from both NaA zeolite layer and PES support; of particular note, progressive blue shift of the Si-O-T band (from 965 to 994 cm^{-1}) revealed the condensation of terminal silanol groups into more rigid framework, implying strong interfacial interactions that restricted polymer chain mobility. The above conclusion could be further supported by elevated glass transition temperature (T_g) observed in DSC analysis. To further gain insights into the interfacial architecture of the obtained NaA zeolite membrane, cross-sectional EDX elemental mapping was performed. As shown in Fig. 2f, while Si element was predominantly located in top dense layer, an obvious infiltration of Si element into porous PES matrix could be clearly observed at the boundary. The above elemental distribution profile provided direct evidence for physical interlocking between NaA zeolite layer and polymer support; in addition, elemental distributions of Al and O exhibited similar interfacial penetration behaviors (Fig. S8), further confirming the formation of a robust interlocked interface rather than simple physical stacking.

3.2. Physicochemical properties of NaA membranes

To further identify the phase purity and chemical composition of obtained NaA zeolite membrane, X-ray photoelectron spectroscopy (XPS) analysis was carried out. Fig. 3c presents the high-resolution normalized XPS spectra of Si 2p and Al 2p regions. The Si 2p spectrum exhibited a symmetrical peak centered at 102.3 eV, which was characteristic of the Si element in a zeolitic Si-O-Al environment. Similarly, the Al 2p spectrum displayed a distinct peak at 74.1 eV, corresponding to tetrahedrally coordinated Al species within the zeolite lattice. The above results convincingly demonstrated the formation of pure NaA zeolite phase on the PES support.

Considering practical operation conditions such as elevated temperature during gas separation, thermal stability of obtained membrane was evaluated through measuring glass transition temperature (T_g) of the samples. As shown in Fig. 3d and S9, the bare PES support exhibited T_g of 229 °C, which was significantly lower than that of PES-supported NaA zeolite membrane (245 °C). The increased T_g can be attributed to reinforced physical interaction between NaA zeolite crystallites and polymer chains of the PES support, resulting in constrained mobility of the underlying polymer segments. The enhanced adhesion between the two phases is crucial for mitigating interfacial stress and therefore, ensuring structural integrity under harsh operation conditions.

In addition to T_g measurement, thermogravimetric analysis (TGA) was further employed to evaluate the intrinsic thermal stability and ascertain the structural decomposition threshold of the composite membrane. As shown in Fig. 3e, obtained membrane did not show significant weight loss until 450 °C. The decomposition mainly occurred at peak temperature of 573 °C as determined from derivative thermogravimetric (DTG) curve (Fig. S10). Through combining with superior interfacial adhesion, our membrane should be adaptable to high temperature and harsh environments; moreover, based on the residual mass of samples at 800 °C, the calculated zeolite loading for PES-supported NaA zeolite membrane reached 45.8 wt%, which was significantly higher than that of the seed layer (11.67 wt%), confirming that the nutrient was mainly consumed in supporting epitaxial growth of the seed layer rather than excessive bulk nucleation and growth in precursor solution, which may promote epitaxial growth and suppress the generation of grain boundary defects in the membrane.

It should be noted that excellent mechanical strength was of vital importance for sustaining membrane operation under harsh conditions. Considering potential benefits derived from flexible PES supports, mechanical properties of obtained NaA zeolite membrane were further tested by tensile measurements. As shown in Fig. 3f, the PES support showed typical elastoplastic behavior with an elongation at break of ~60%; in comparison, the maximum tensile strength decreased from 46.6 MPa for the bare PES support to 29.5 MPa for the PES-supported NaA zeolite membrane, corresponding to the retention of 63.5% of tensile strength. Nonetheless, this value remained remarkably higher than brittle ceramic supports (typically <0.1%), which was crucial for preventing catastrophic fracture during handling and module assembly. As a proof of concept, repetitive bending tests were performed. As shown in Fig. S11, even after 20 bending cycles, the NaA zeolite layer remained

well-intergrown and firmly attached to the support, which was indicative of robust interfacial interlocking. After wetting and drying, the membrane largely retained its H_2/CO_2 separation performance (Fig. S12). To the best of our knowledge, the successful fabrication of a highly flexible NaA zeolite membrane with such exceptional bending durability has not been reported in previous literature.

3.3. Gas separation performance

Gas permeation properties of the as-synthesized membrane were evaluated using a Wicke-Kallenbach setup (Fig. S13). We first tested the permeation behavior of single gases (i.e., H_2, CO_2, CH_4, SF_6, and N_2) at 298 K. As shown in Fig. 4a, gas permeance sharply decreased with increasing kinetic diameter, following the order $H_2 > N_2 \approx CO_2 > CH_4 > SF_6$. This cut-off behavior indicates that molecular sieving is the dominant separation mechanism. Of particular note, its H_2 and N_2 permeances reached 2.97×10^{-6} and 2.95×10^{-7} mol m^{-2} s^{-1}·Pa^{-1}, respectively, corresponding to an ideal H_2/N_2 selectivity of 10.1, which is 2.7 times higher than the corresponding Knudsen selectivity of 3.73. The above results further support the presence of few non-selective grain boundary defects in the membrane. The membrane also exhibited an ideal H_2/CO_2 selectivity of 10.26, demonstrating a favorable combination of H_2 permeance and molecular selectivity.

We further investigated mixed gas permeation properties of the membrane. As shown in Fig. 4b, the SF of equimolar H_2/CO_2 gas pair reached 15.7 with H_2 permeance of 2.6×10^{-6} mol m^{-2} s^{-1}·Pa^{-1}, which was higher than the corresponding ideal selectivity. This could be attributed to a significant competitive adsorption effect. To be specific, since the NaA zeolite framework possessed much stronger adsorption affinity for CO_2 than H_2, upon mixing, CO_2 molecules preferentially occupied the adsorption sites within the zeolite channels, creating a "site-blocking effect" that curtailed the available diffusion space. Notably, while the presence of adsorbed CO_2 imposed certain resistance to H_2 transport, the mobility of CO_2 itself was more severely retarded due to its larger kinetic diameter and stronger interaction with zeolite pore walls, resulting in enhanced H_2/CO_2 SF compared with the corresponding ideal selectivity [50]. The above competitive adsorption mechanism can be supported by CO_2 adsorption isotherms of NaA zeolite powders (Fig. S6), revealing a steep uptake in the low-pressure region and remarkably high CO_2 capacity (~120 cm^3 g^{-1} STP, or 5.34 mmol g^{-1}, at 1 bar) indicative of strong affinity of NaA zeolite framework for CO_2 molecules.

Considering the significant influence of operation temperature, its effect on the H_2/CO_2 separation performance of our membrane was studied further. As shown in Fig. 4c, upon increasing temperature from 298 K to 423 K, its H_2 permeance steadily increased from 2.6×10^{-6} to 4.0×10^{-6} mol m^{-2} s^{-1}·Pa^{-1}, while the CO_2 permeance more pronouncedly increased from 1.7×10^{-7} to 5.8×10^{-7} mol m^{-2} s^{-1}·Pa^{-1}, causing a decrease of SF from 15.7 to 7.0. This is rational, since smaller-sized H_2 molecules have a lower activation energy for diffusion through zeolite pores compared with larger-sized CO_2 molecules; as a result, the permeance of CO_2 was more sensitively influenced by operation temperature, ultimately leading to lower H_2/CO_2 SF. In effect, the above temperature-dependent behavior was also observed in terms of H_2/CH_4 and H_2/SF_6 separations (Fig. S14). From an economic viewpoint, elevating operation temperature was more advantageous, since reduced membrane area was required to achieve the same production target on the premise that the product purity could be fully met.

Finally, the operational stability of the PES-supported NaA zeolite membrane was evaluated for 40 h. Experimental results indicated that both H_2 permeance and H_2/CO_2 SF remained nearly constant during the 40 h continuous test (Fig. 4d). The stable performance could be further confirmed by H_2/CH_4 and H_2/SF_6 separations (Fig. S15). In addition, mechanical robustness of our membrane was verified by the bending test. As shown in Fig. S11, our membrane retained stable H_2/CO_2 SF of 15.5 with no significant degradation even after being subjected to repeated bending cycles. This could be attributed to the high flexibility

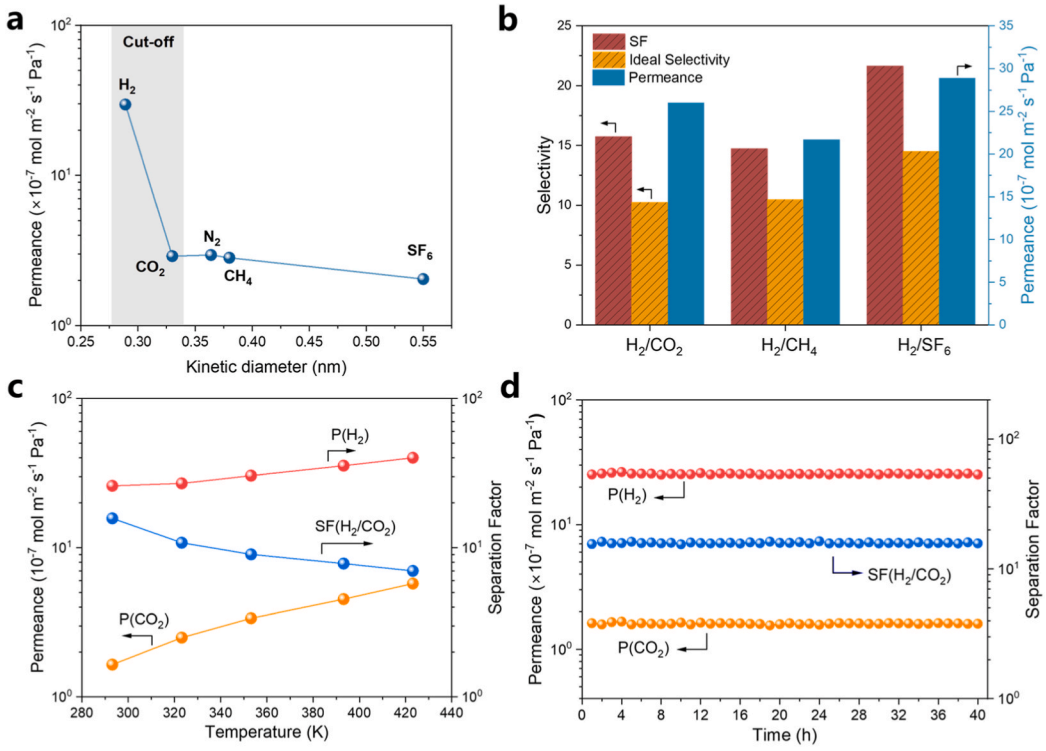


Fig. 4. (a) Single-gas permeance as a function of kinetic diameters of gas molecules. (b) Separation performances of PES-supported NaA zeolite membrane. (c) Dependence of operation temperature on H_2/CO_2 separation performance. (d) 40-h stability test of the membrane for H_2/CO_2 separation. Unless otherwise specified, all mixed-gas measurements were performed at 298 K with an equimolar feed under transmembrane partial pressure difference of 1 bar.

of polymer supports, enabling efficient strain force transfer from brittle NaA zeolite layer to PES support once an external stress was exerted. Obviously, enhanced mechanical stability of our membrane was advantageous for preventing structural fracture formation during large-scale module assembly and enduring mechanical vibrations under practical operating conditions.

To fully evaluate the performance superiority of our membrane in terms of H_2/CO_2 separation, its performance was compared with representative H_2-permselective zeolite membranes, polymer membranes, and mixed-matrix membranes (MMMs). As illustrated in Fig. 5, in comparison with the literature, the PES-supported NaA membrane exhibits ultrahigh H_2 permeance while maintaining competitive H_2/CO_2 SF (Table S1). The ultrahigh H_2 permeance as well as excellent H_2/CO_2 and H_2/CH_4 selectivity can be attributed to the low diffusion resistance of the PES support and the presence of few intercrystalline defects in well-intergrown NaA zeolite layer. In addition, the flexibility of the PES support may help accommodate stress generated during membrane growth, thereby preserving the integrity of the zeolite selective layer. It is therefore anticipated that cost-effective H_2 purification on an industrial scale can be realized through concurrently maximizing processing capacity and minimizing capital cost.

3.4. Cost-benefit analysis

To quantitatively assess the industrial viability of our membrane, an initial economic evaluation [51] was conducted based on a standardized hydrogen production task of 100 kg per day (0.5741 mol s^{-1}) operating at 298 K with a transmembrane pressure drop of 1 bar. For comparison, representative porous α-Al_2O_3-supported NaA zeolite membranes were deliberately selected and evaluated following a similar protocol. As shown in Fig. 6a, since our membrane exhibited much higher H_2 permeance, compared with other ceramic-supported counterparts with required membrane areas up to 35.9 m^2, a much smaller membrane area of only 2.2 m^2 was sufficient to achieve the target productivity. It should be noted that reducing the membrane area not only lowers the support cost but also implies a proportional decrease in the consumption of reagents and energy input during membrane processing, jointly contributing to the overall economic viability.

Based on required membrane areas, a total fabrication cost comprising both supports and selective layers was calculated. As shown in Fig. 6b, compared with conventional ceramic-supported counterparts in the range of 3940 to 59,236 USD, the total cost for PES-supported NaA zeolite membrane was only 421 USD, which was equivalent to 89.3-99.2% reduction in total fabrication cost, demonstrating exceptional economic competitiveness. The substantial cost reduction can be interpreted as follows: On the one hand, the cost of commercial PES supports is ~97.2% lower than commercial ceramic supports (SI-Cost-Benefit Analysis); on the other hand, significantly reduced membrane area (Fig. 6a) results in lower consumption for fabricating qualified NaA zeolite layers.

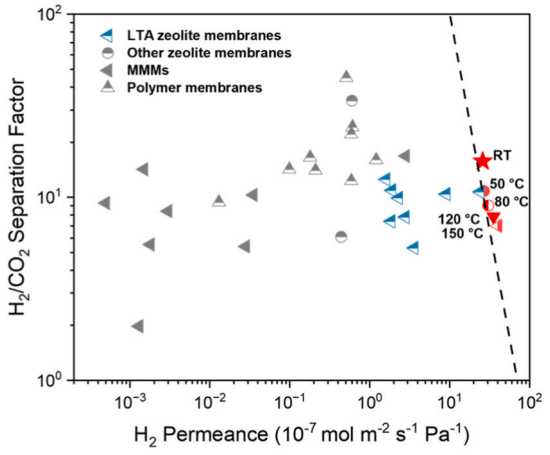


Fig. 5. Comparison of the H_2/CO_2 separation performance of PES-supported NaA zeolite membrane with other H_2-permselective membranes reported in the literature. The red symbols denote the separation performance of our membrane at different operation temperatures.

Besides economic viability analysis at room temperature, H_2/CO_2 separation performances of our membranes at varying temperatures (20-150 °C) were further compared with literature benchmarks. As shown in Fig. 6c and d, H_2 permeance of our membrane was positively associated with operation temperature and remained the highest among the above membranes under identical operating temperatures, while its H_2/CO_2 SF remained competitive, demonstrating its great potential in high-efficiency H_2 purification from industrial off-gases under practical conditions.

3.5. Generality of the fabrication strategy

To verify the versatility and broad applicability of the above synthetic strategy, we further fabricated PES-supported MFI zeolite membrane through mild epitaxial growth. As shown in Fig. 7a, after hydrothermal reaction at 90 °C for 15 h, a uniform and well-intergrown MFI zeolite layer was readily formed on the PES support (Fig. 7b). Cross-sectional SEM image clearly revealed a distinct and compact zeolite layer tightly adhered to the porous PES matrix, confirming the formation of a robust interface between them (Fig. 7c). The formation of pure-phase MFI zeolite membrane could be further validated by relevant XRD pattern, in which the characteristic diffraction peaks of the newly formed MFI phase completely masked the amorphous hump of the PES support (Fig. 7d). We therefore conclude that adopting cheap commercial polymer supports represents a promising solution to large-scale fabrication of cost-effective zeolite membranes with optimized microstructures towards superior separations.

4. Conclusions

In this study, we developed a facile and scalable strategy to fabricate high-performance, flexible NaA zeolite membranes on low-cost commercial PES supports. Through employing a vacuum hot-drop coating method, controlled physical anchoring of zeolite seeds in macropores of the support can be achieved, ensuring the formation of a continuous and well-intergrown NaA zeolite layer with strong and robust interfacial adhesion. As-prepared membrane exhibits ultrahigh H_2 permeance (~2.6 × 10^{-6} mol m^{-2} s^{-1}·Pa^{-1}) as well as high SF for H_2/CO_2 (15.7) and H_2/CH_4 (14.7) gas pairs, which is superior to the majority of H_2-permselective membranes reported in the literature. Furthermore, our membrane demonstrates high thermal stability and stable separation performance over 40 h. A comprehensive cost-benefit analysis further reveals that a total reduction in fabrication cost by 89.3-99.2% is achieved in comparison with ceramic-supported counterparts. The above strategy can be further generalized to the preparation of PES-supported MFI zeolite membranes, demonstrating its great potential in cost-effective production of versatile molecular sieve membranes.

CRediT authorship contribution statement

Shijie Yang: Writing – original draft, Methodology, Investigation, Formal analysis, Data curation, Conceptualization. **Jiahong Pan:** Supervision, Funding acquisition, Conceptualization. **Yi Liu:** Supervision, Funding acquisition, Conceptualization. **Shengyan Meng:** Data curation. **Hongyan Xiao:** Formal analysis. **Yunlei Gao:** Formal analysis. **Junze Li:** Data curation. **Weijun Xu:** Formal analysis. **Minxiu Zou:** Formal analysis. **Meng Ge:** Supervision, Resources. **Rongfei Zhou:** Formal analysis. **Yi Liu:** Supervision, Funding acquisition, Conceptualization.

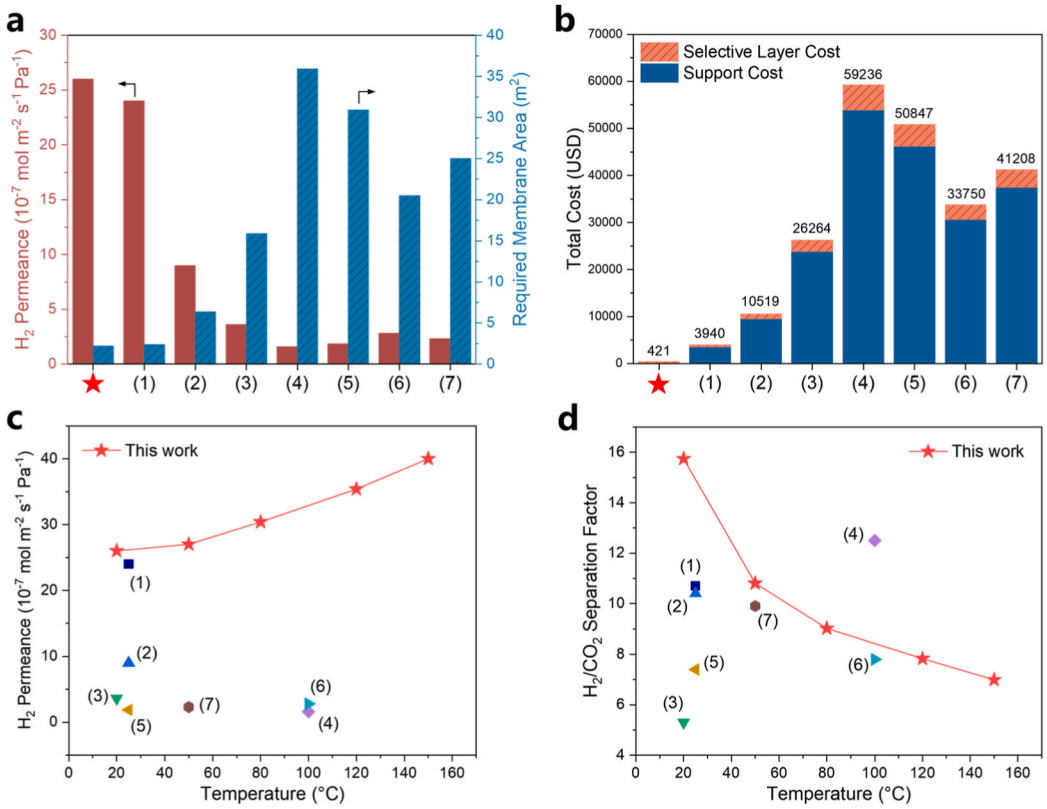


Fig. 6. (a) Comparison of H_2 permeance and calculated membrane area required for standardized industrial task. The red star represents this work, while (1) - (7) denote literature benchmarks (details are provided in Table S1). (b) Performance-normalized cost-benefit analysis. Temperature-dependent comparison of (c) H_2 permeance and (d) H_2/CO_2 SF of PES-supported NaA zeolite membrane with the literature.

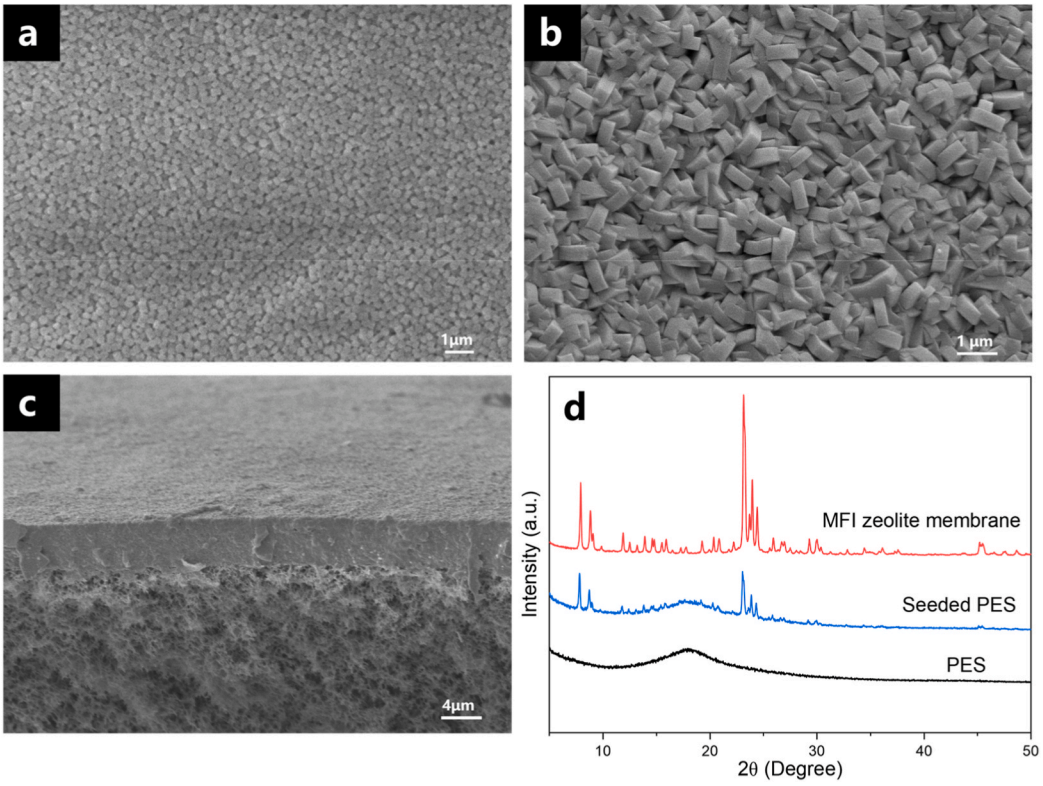


Fig. 7. (a) SEM image of MFI zeolite seed layer. (b, c) SEM images of PES-supported MFI zeolite membrane. (d) XRD patterns of bare PES support, MFI zeolite seed layer, and PES-supported MFI zeolite membrane.

Declaration of competing interest

The authors declare that they have no known competing financial interests or personal relationships that could have appeared to influence the work reported in this paper.

Acknowledgements

Y.L. acknowledges the funding from National Key Research and Development Program of China (2023YFB3810700), National Natural Science Foundation of China (22461142141, 22478056, 22078039 and 22578043), Science and Technology Innovation Fund of Dalian (2024JJ12GX027), and Fundamental Research Funds for the Central Universities (DUT22LAB602) for the financial support.

Appendix A. Supplementary data

Supplementary data to this article can be found online at https://doi.org/10.1016/j.memsci.2026.126220.

Data availability

The authors do not have permission to share data.

References

[1] K. Alanazi, S. Mittal, A. Hawkes, N. Shah, Renewable hydrogen trade in a global decarbonised energy system, Int. J. Hydrogen Energy 101 (2025) 712–730.
[2] S. Algburi, H. Munther, O. Al-Dulaimi, H.F. Fakhruldeen, I.B. Sapaev, K.F.K. A. Seedi, D.H. Khalaf, F.I. Jabbar, Q. Hassan, A. Khudhair, G. Nakimera, Green hydrogen role in sustainable energy transformations: a review, Results Eng. 26 (2025) 105109.
[3] M.A. Elazab, A.T. Elgohr, M. Bassyouni, A.E. Kabeel, M.E.H. Attia, M. K. Elshaarawy, A.K. Hamed, H.A.H. Alzahrani, Green hydrogen: unleashing the potential for sustainable energy generation, Results Eng. 27 (2025) 106031.
[4] X. Chen, F. Niu, T. Ma, Q. Li, S. Wang, S. Shen, Anchoring group regulation in semiconductor/molecular complex hybrid photoelectrode for photoelectrochemical water splitting, Smart Molecules 3 (2025) e20240056.
[5] L. Zheng, S. Ju, S. Fang, H. Zhang, Z. Cai, K. Huang, L. Jiang, Rational design of deep eutectic solvents with low viscosities and multiple active sites for efficient recognition and selective capture of NH_3, Smart Molecules 3 (2025) e20240045.
[6] H. Ju, Y. Zhang, J. Zhang, Z. Yu, Y. Zhang, X. Zhang, X. Guo, J. Liu, Q. Mao, Q. Liu, Y. Zhao, T. Qi, X. Jiang, Z. Guo, S. Chen, Development of a novel Cu(I) π-complexation adsorbent for ultra-deep desulfurization from a carbon dioxide stream, Smart Molecules 3 (2025) e20240027.
[7] Y. Sun, Y. Liu, J. Caro, X. Guo, C. Song, Y. Liu, In-Plane epitaxial growth of highly c-Oriented NH_2-MIL-125(Ti) membranes with superior H_2/CO_2 selectivity, Angew. Chem. Int. Ed. 57 (2018) 16088–16093.
[8] S. Chen, M. Wahiduzzaman, T. Ji, Y. Liu, Y. Li, C. Wang, Y. Sun, G. He, G. Maurin, S. Wang, Y. Liu, Oriented Titanium-MOF membrane for hydrogen purification, Angew. Chem. Int. Ed. 64 (2025) e202413701.
[9] S. Duan, H. Xu, J. Zhang, M. Shan, S. Zhang, Y. Zhang, X. Wang, F. Kapteijn, Benzimidazole-linked polymer membranes for efficient syngas ($H_2/CO/CO_2$) separation, J. Membr. Sci. 717 (2025) 123595.
[10] S. Jia, J. Tan, Z. Zhou, S. Zhang, A sustainable method to prepare ultra-thin MOF hollow fiber membranes for H_2 separation, J. Membr. Sci. 721 (2025) 123794.
[11] F. Jiang, J. Yang, M. Yan, Enhancement strategy for superior H_2/CO_2 separation with binary Ag-MgO doped silica membranes, J. Membr. Sci. 734 (2025) 124392.
[12] Y. Shen, F. Jiang, Q. Liu, Z. Chen, K. Ge, J. Bai, J. Duan, Size effect of porous filler in mixed matrix membranes for faster hydrogen permeation from methane-containing mixtures, Adv. Membr. 5 (2025) 100136.
[13] H. Wang, C. Zhang, L. Fan, Z. Kang, D. Sun, Combining zeolite with MOF glass to construct crystal-glass composite membranes for improved hydrogen separation, Adv. Membr. 5 (2025) 100164.
[14] W. Lim, W. He, J. Ma, S.U. Hassan, J. Du, Q. Sun, D. Cao, J. Guan, H. Zhang, J. Liu, Membranes with hollow bowl-shaped window for CO_2 removal from natural gas, Adv. Membr. 5 (2025) 100129.
[15] Y. Zhang, C. Liang, Z. Li, X. Li, Anchoring metal ions in iCOF to enhance the charge density for boosting CO_2 separation in mixed matrix membranes, Adv. Membr. 5 (2025) 100167.
[16] T. Xia, Y. Wu, T. Ji, W. Hu, K. Yu, X. He, B.H. Yin, Y. Liu, Mixed-matrix membranes incorporating hierarchical ZIF-8 towards enhanced CO_2/N_2 separation, Smart Molecules 3 (2025) e20240066.
[17] R.W. Baker, B.T. Low, Gas separation membrane materials: a perspective, Macromolecules 47 (2014) 6999–7013.
[18] N. Rangnekar, N. Mittal, B. Elyassi, J. Caro, M. Tsapatsis, Zeolite membranes – a review and comparison with MOFs, Chem. Soc. Rev. 44 (2015) 7128–7154.
[19] C. Huang, C. Zuo, X. Chen, W. Xing, Research progress and challenges in polyimide and polyimide-derived gas separation membranes: a review, Adv. Membr. 5 (2025) 100154.
[20] R. Bedard, C. Liu, Recent advances in zeolitic membranes, Annu. Rev. Mater. Res. 48 (2018) 83–110.
[21] Y. Liu, Y. Li, W. Yang, Fabrication of highly b-oriented MFI film with molecular sieving properties by controlled in-plane secondary growth, J. Am. Chem. Soc. 132 (2010) 1768–1769.
[22] Y. Liu, W. Qiang, T. Ji, M. Zhang, M. Li, J. Lu, Y. Liu, Uniform hierarchical MFI nanosheets prepared via anisotropic etching for solution-based sub-100-nm-thick oriented MFI layer fabrication, Sci. Adv. 6 (2020) eaay5993.
[23] Y. Liu, S. Chen, T. Ji, J. Yan, K. Ding, S. Meng, J. Lu, Y. Liu, Room-temperature synthesis of zeolite membranes toward optimized microstructure and enhanced butane isomer separation performance, J. Am. Chem. Soc. 145 (2023) 7718–7723.
[24] M. Sakai, Y. Koshiishi, A. Okada, K. Kawanishi, K. Masuda, M. Matsukata, A review of strategies for developing zeolite membranes: from a microstructure to a membrane module, Cryst. Growth Des. 25 (2025) 5584–5620.
[25] D. Gai, Y. Guan, D. Ma, Y. Deng, J. Dong, Z. Wang, J. Li, I. Agirrezabal-Telleria, X. Zou, Co-exchanged SSZ-13 zeolite membrane for boosting CO_2/N_2 separation, J. Membr. Sci. 722 (2025) 123874.
[26] Y. Liu, W. Qiang, J. Lu, Y. Liu, Fabrication of highly a-oriented ultrathin FER zeolite membrane from nanosheets towards small-sized gas separation, J. Membr. Sci. 734 (2025) 124437.
[27] L. Peng, L. Zhao, G. Pan, X. Gu, Synthesis of tungsten-doped MFI zeolite membranes with improved performance for CO_2/N_2 separation, J. Membr. Sci. 729 (2025) 124185.
[28] D. Li, M. Ye, C. Ma, N. Li, Z. Gu, Z. Qiao, Preparation of a self-supported zeolite glass composite membrane for CO_2/CH_4 separation, Smart Molecules 2 (2024) e20240009.
[29] H. Li, C. Qiu, S. Ren, Q. Dong, S. Zhang, F. Zhou, X. Liang, J. Wang, S. Li, M. Yu, Na +-gated water-conducting nanochannels for boosting CO_2 conversion to liquid fuels, Science 367 (2020) 667–671.
[30] A. Huang, F. Liang, F. Steinbach, T.M. Gesing, J. Caro, Neutral and cation-free LTA-type aluminophosphate ($AlPO_4$) molecular sieve membrane with high hydrogen permselectivity, J. Am. Chem. Soc. 132 (2010) 2140–2141.
[31] F.J. Varela-Gandía, A. Berenguer-Murcia, D. Lozano-Castelló, D. Cazorla-Amorós, Hydrogen purification for PEM fuel cells using membranes prepared by ion-exchange of Na-LTA/carbon membranes, J. Membr. Sci. 351 (2010) 123–130.
[32] C. Xu, W. Wei, Y. He, Enhanced hydrogen separation performance of linde Type-A zeolite molecular sieving membrane by cesium ion exchange, Mater. Lett. 324 (2022) 132680.
[33] Z. Dong, Z. Wang, L. Zhang, Q. Fu, M. Wang, Competitive adsorptive mechanism of H_2/N_2 in LTA/FAU zeolites by molecular simulations and experiments, Molecules 29 (2024) 3686.
[34] P. Yu, G. Yang, Y. Chai, L. Tosheva, C. Wang, H. Jiang, C. Liu, H. Guo, Self-limiting growth of thin dense LTA membranes boosts H_2 gas separation performance, Chem. Eng. J. 479 (2024) 147629.
[35] Y. Gao, M. Ge, S. Tao, Y. Liu, S. Meng, K. Yu, J. Yan, M. Wu, K. Ding, X. He, W. Dong, Y. Liu, Near-ambient temperature synthesis of NaA zeolite membranes towards high-efficiency ethanol dehydration pervaporation and ammonia separation, J. Membr. Sci. 749 (2026) 125409.
[36] F.Z. Charik, B. Achiou, A. Belgada, Z.C. Elidrissi, M. Ouammou, M. Rabiller-Baudry, S.A. Younssi, Optimal preparation of low-cost and high-permeation NaA zeolite membrane for effective ethanol dehydration, Microporous Mesoporous Mater. 344 (2022) 112229.
[37] Z. Huang, T. Wu, J. Zeng, Z. Sun, S. Xiong, L. Zhang, B. Liu, M. Zhu, F. Zhang, X. Chen, H. Kita, Efficient preparation of large-area, high-selective SSZ-13 membrane, J. Membr. Sci. 734 (2025) 124456.
[38] J.-B. Zhang, Q. Liu, W.-Y. Pan, J.-W. Wu, X. Li, M. Pan, Z.-S. Shi, C.-L. Du, X.-L. Wei, Support-layer integrated zeolite membranes through in situ interfacial transformation of clay-based protomembranes, Angew. Chem. Int. Ed. 64 (2025) e202420696.
[39] I.G. Wenten, P.T. Dharmawijaya, P.T.P. Aryanti, R.R. Mukti, K. Khoiruddin, LTA zeolite membranes: current progress and challenges in pervaporation, RSC Adv. 7 (2017) 29520–29539.
[40] F. Kapteijn, X. Wang, Zeolite membranes – the importance of support analysis, Chem. Ing. Tech. 94 (2022) 23–30.
[41] H. Guo, W. Xu, J. Wei, Y. Ma, Z. Qin, Z. Dai, J. Deng, L. Deng, Effects of porous supports in thin-film composite membranes on CO_2 separation performances, Membranes 13 (2023) 359.
[42] X. Jin, S. Wang, Y. Zhao, L. Liu, X. Gao, X. Gu, Analysis of the gas transport resistance of CO_2 and CH_4 through ultra-thin DD3R zeolite membrane, J. Membr. Sci. 706 (2024) 122929.
[43] Q. Ge, Z. Wang, Y. Yan, High-performance zeolite NaA membranes on polymer-zeolite composite hollow fiber supports, J. Am. Chem. Soc. 131 (2009) 17056–17057.
[44] M. Severance, B. Wang, K. Ramasubramanian, L. Zhao, W.S.W. Ho, P.K. Dutta, Rapid crystallization of faujasitic zeolites: mechanism and application to zeolite membrane growth on polymer supports, Langmuir 30 (2014) 6929–6937.
[45] M. Dakhchoune, X. Duan, L.F. Villalobos, C.E. Avalos, K.V. Agrawal, Hydrogen-sieving zeolitic films by coating zeolite nanosheets on porous polymeric support, J. Membr. Sci. 672 (2023) 121454.
[46] Y. Deng, F. Qiu, J. Wu, J. Li, Z. Li, Q. Huang, G. Zhu, X. Zou, Flexible ZSM-5 zeolite membrane for high-performance helium separation, Angew. Chem. Int. Ed. 64 (2025) e202421285.

[47] H. Hong, K. Yu, H. Liu, R. Zhou, W. Xing, Industrial-scale 61-channel monolithic silicalite-1 membranes for butane isomer separation, Adv. Membr. 4 (2024) 100096.
[48] S.G. Chaudhri, P.S. Singh, In situ hydrothermal growth of Zeolite-A membrane on polysulfone hollow fibers, Microporous Mesoporous Mater. 366 (2024) 112952.
[49] B. Wang, P.K. Dutta, Influence of cross-linking, temperature, and humidity on CO_2/N_2 separation performance of PDMS coated zeolite membranes grown within a porous poly(ether sulfone) polymer, Ind. Eng. Chem. Res. 56 (2017) 6065–6077.
[50] K. Xu, C. Yuan, J. Caro, A. Huang, Silver-exchanged zeolite LTA molecular sieving membranes with enhanced hydrogen selectivity, J. Membr. Sci. 511 (2016) 1–8.
[51] P. Du, X. Cui, J. Zhang, Y. Ren, H. Liu, Y. Zhang, X. Gu, Techno-economic evaluation of hollow fiber DD3R zeolite membrane module for hydrogen extraction from hydrogen-blended natural gas, J. Membr. Sci. 722 (2025) 123877.